Advances in Aircraft and Spacecraft Science, *Vol. 5, No. 5 (2018) 551-579*
DOI: https://doi.org/10.12989/aas.2018.5.5.551

On determining the flyability of airplane rectilinear trajectories at constant velocity

Gilles Labonté*

Department of Mathematics and Computer Science, Royal Military College of Canada, Kingston, Ontario, Canada

(Received January 23, 2018, Revised March 4, 2018, Accepted March 5, 2018)

Abstract. This work is concerned with the motion of propeller driven airplanes, flying at constant velocity on ascending or descending rectilinear trajectories. Its purpose is to provide important features of rectilinear flights that are required for airplane trajectory planning but that cannot be found already published. It presents a method for calculating the amount of fuel used, the restrictions on the trajectory parameters, as inclination and speed, which result from the load factor, the lift coefficient, the positivity and upper boundedness of the power available. It presents a complete discussion of both ascending and descending flights, including gliding. Some original remarks are made about the parameters of gliding. It shows how to construct tables of parameters allowing to identify rapidly flyable trajectories. Sample calculations are shown for the Cessna 182 and a Silver Fox like unmanned aerial vehicle.

Keywords: airplane rectilinear trajectory; inclined rectilinear motion, airplane equation of motion; automatic trajectory planning; gliding

1. Introduction

This study is motivated by the need to provide automatic trajectory planning for rendering unmanned aerial vehicles (UAVs) autonomous. UAVs, flying in a cluttered environment or mountainous terrain, are required to calculate new flyable trajectories when there happens unforeseen obstacles or changes in the environment or in the mission. Essential tools for performing this task are formulas or tables that indicate what trajectories are flyable by the airplane in question. The determination of the flyability of trajectories has to take into account the particular dynamics of the airplane and provide basic information such as the amount of fuel required, the time of flight, etc. The results obtained in this study are actually quite general and constitute important tools not only for UAV trajectory planning, but also for the analysis of the motion of all propeller driven airplanes.

An efficient technique for constructing trajectories was proposed by Frazzoli *et al*. (2005). It consists in concatenating elementary trajectory segments, called motion primitives, taken from a finite library. The primitives most often considered are rectilinear, circular and helical segments. Their properties could be calculated in advance and stored in the memory of the airplane computing device. The main advantage of this approach is the minimization of the calculations

*Corresponding author, Emeritus Professor, E-mail: gilles.labonte@rmc.ca

http://www.techno-press.org/?journal=aas&subpage=7 ISSN: 2287-528X (Print), 2287-5271 (Online)

required since then only the connection between the segments have to be calculated. A somewhat similar, often used, approach consists in firstly building a skeleton trajectory made up of connected rectilinear segments and then smoothing out the connections because the velocity is necessarily continuous. This smoothing can be done with splines, as described in, among others, Judd (2001), Zheng *et al*. (2003), Nikolos *et al*. (2003), Yang and Sukkarieh (2010), Jiabo *et al*. (2012), Wang *et al*. (2017). However, splines are not readily analyzable for flyability, whether they constitute connection segments or even the whole trajectory as in Holub *et al*. (2012), Neto *et al*. (2013), Askari *et al*. (2015).

A more manageable method is often preferred for connecting rectilinear segments: it is done with arcs of circles or helices. This approach was initiated by Dubins (1957) and further developed by Chandler *et al*. (2000), Jia and Vagners (2004), Chitsaz and LaValle (2007), Hwangbo *et al*. (2007), Allaire *et al*. (2009), Li Xia *et al*. (2009), Ambrosino *et al*. (2009), Babaei and Mortazavi *(2010)*, Hota and Ghose (2010, 2014), Roberge *et al*. (2012), Niendorf *et al*. (2013), Xian-Zhong *et al*. (2013), Weiwei *et al*. (2014), Zhu Wang *et al*. (2014), Rudnick-Cohen *et al*. (2015), Ramana *et al*. (2016), Kok and Rajendran (2016).

Essentially all studies on airplane trajectory planning, except for Roberge *et al*. (2012) are done with a version of the Dubins (1957) airplane model that incorporates, at best, oversimplified constraints on the speed, on the angle of climb and on the turning radius of the airplane, which are considered constant everywhere on the trajectory. In reality, however, all these parameters depend very strongly on the altitude and on the inclination of the trajectory and this fact has to be taken into account. For example, from Labonté (2016), one can calculate that for a Silver Fox UAV, that flies on a circular trajectory, inclined at 10° with the horizon, at the speed of 20 m/s, the minimum turning radius is 13.9 m, while, if its speed is 35 m/s, its turning radius is 39.3 m. When it flies on a horizontal circular trajectory at a speed of 20 m/s, its minimum turning radius at sea level is 13.1 m, while at an altitude of 3000 m, it is 18.5 m. The possible speeds at which an airplane can fly evidently depend on the altitude and the inclination of the trajectory. To obtain a realistic trajectory planner, it is necessary to take into account all the constraints imposed by the airplane dynamics. This is done in the present work, which is based on the realistic airplane model described in Anderson (2000). We note that we also use the same nomenclature as in Anderson (2000).

We note that, even after the smoothing process of the trajectory is performed, most of it still consists of rectilinear segments. When the terrain is uneven or there are many obstacles and the UAV must fly as low as possible, there will be many climbing and descending rectilinear segments, together with some horizontal segments. It is therefore of outmost importance to be able to determine all the features of these important pieces of trajectory. The motion of airplanes on horizontal rectilinear trajectories is discussed in most books on airplane dynamics; see for example Hale (1984), Anderson (2000), Eshelby (2000), Yechout *et al*. (2003), Stengel (2004) and Filippone (2006). Climbing flights are also most of the time discussed. However, in our survey of many classical airplane dynamics books, we did not find any that provides a complete solution to the climbing flight equations. The discussions usually only deal with instantaneous aspects of the climbing flight, never with the entire flight. For example, Yechout *et al*. (2003) simply define the local climbing rate and, Torenbeek (1976), Hale (1984), Anderson (2000), Eshelby (2000), Stengel (2004) and Filippone (2006) all derive conditions for the instantaneous climbing angle or climbing rate to be maximum. These conditions are obtained by calculating the derivative of some expression with respect to the speed or the lift coefficient, while considering as constant all the other variables such as the air density, the temperature and the airplane weight. This process yields formulas that cannot be satisfied for the entire trajectory, as the values of these parameters change

in time. Thus, airplane dynamics books provide no global solution for the time evolution of the lift, the power and the fuel required when an airplane travels an entire climbing or descending trajectory. The inadequacy of this approach is recognized in Section 2.6 of Stengel (2004) and in Section 8.6 of Filippone (2006), who mention that such steady state models cannot be correct because the climbing rate and the optimal climbing conditions change with changing altitude so that the airplane in fact accelerates. Furthermore, in all the airplane dynamics books that we have examined, the climbing and descending flights are always considered to make an inclination angle θ, with the horizontal, that is small so that $\cos(\theta) \approx 1$. This may be justified for most commercial propeller-driven airplanes, for which θ is at most about 10°-15°, but it is not true for fighter airplanes and UAVs. The latter airplanes can fly much bolder manoeuvres than inhabited propeller airplanes. In the present study, we do not make this approximation of small angles; all the formulas we derive are applicable for any angle of climb and descent.

Exact formulas and very accurate approximation formulas for the amount of fuel used for inclined rectilinear trajectories were first presented in Labonté (2012, 2015). These studies concentrated on that particular aspect of the flight and did not analyse the constraints on the trajectories that are imposed by the dynamical abilities of the airplane. The purpose of the present article is to complement these results by determining all these constraints. The dynamical parameters considered are the airplane load factor, its lift coefficient, its available power and the discussion takes into account the influence of altitude.

We recall from Chapter 9 of Anderson (2000) that the power P_R that is required for the motion of a propeller driven airplane is derived from the power P_P produced by its engine as $P_R = \eta P_P$ in which η is the propeller efficiency. The rate of fuel burning is given by

$$\frac{dW}{dt} = -c P_P = -\frac{c}{\eta} P_R \tag{1}$$

in which W is the weight of the airplane and c is the specific fuel consumption. We shall consider that the thrust produced by the propeller T_R is along the direction of the airplane motion, so that $P_R = V_\infty T_R$. It is important to take into account that the power produced by a combustion engine varies with the altitude; that is

$$P_P(h) = P_P(0)\frac{\rho(h)}{\rho_s} \tag{2}$$

For simplicity, in the present study, we consider only flights below 11 km, so that a_1, the rate of variation of the temperature with the altitude, is constant, with

$$T(h) = T_s - a_1 h, \qquad \text{with } a_1 = 6.5 \times 10^{-3}$$

The results we obtain can be readily generalized to flights at higher altitudes by solving the equations of motion inside each traversed zone of the atmosphere, in which the temperature gradients differ and then matching continuously the solutions at the zone boundaries.

The article is organized as follows. It begins by recalling the concepts of power available and power required and the formula for the fuel consumption. It then presents a description of constant velocity rectilinear trajectories and recalls the Newton equation of motion for an airplane of varying mass on such a trajectory. Expressions are obtained for the load factor, the lift coefficient and the limits on the trajectory parameters that result from their being bounded are derived. The non-linear differential equation for the airplane weight is recalled, together with a method for

calculating its solution. Conditions are derived to ensure the non-negativity and the sufficiency of the power required for the motion. Ascending trajectories are examined and a method is obtained to ascertain their flyability. Non-ascending trajectories are then examined along the same lines. It is shown how tables of parameters can be constructed to sum up results that may be rapidly needed in a mission. Some remarks are made about gliding, which is a particularly important type of descending trajectory. The application of the formulas derived is illustrated with airplanes that have similar properties as the following well known two different airplanes:

- the Cessna 182 Skylane, which has a reciprocating engine with a constant speed propeller
- a Silver Fox like unmanned aerial vehicle (UAV) which has a reciprocating engine with a fixed pitch propeller

The required characteristics of these airplanes are listed in Appendix A. There may be small differences between the values we use and the actual values for a particular model of these airplanes. We used values that were readily available on the internet and those that were not, were estimated from the values for similar airplanes. This is adequate for our purpose which is to illustrate the calculations involved in the formulas we derive.

2. Description of constant velocity rectilinear trajectories

Rectilinear segments are the most important constituents of automatically constructed airplane trajectories. These segments link an initial position $\boldsymbol{x}_i$ to a final position $\boldsymbol{x}_f$. Their flyability has to be assessed and if it is flyable, the weight of fuel required to fly it has to be calculated. The airplane is considered to fly at the constant velocity $\boldsymbol{v}$, with $||\boldsymbol{v}|| = V_\infty$ on this segment. In order to simplify the notation, we select the coordinate system such that the rectilinear segment lies in the x-z plane, with $\boldsymbol{x}_i$ at the origin of the x-z plane, at the altitude h_i. We shall consider that $x_f > x_i$. The position of the center of mass of the airplane is then described by

$$\mathbf{x}(t) = \left[0, 0, h_i\right] + V_\infty \left[\cos(\theta), 0, \sin(\theta)\right] t$$

in which θ is the angle that the trajectory makes with a horizontal plane. If the trajectory is ascending, $\theta > 0$ and if it is non-ascending, $\theta \leq 0$. In all cases, $0 \leq |\theta| \leq \pi / 2$. The velocity on this trajectory is

$$\mathbf{v}(t) = V_\infty \left[\cos(\theta), 0, \sin(\theta)\right]$$

Since the lift has to cancel the component of the weight perpendicular to the trajectory, the following transversal equilibrium condition must be satisfied:

$$L = W \cos(\theta) \quad \text{in which} \quad L = \frac{1}{2} \rho_\infty S C_L V_\infty^2 \tag{3}$$

The sum of forces that act in the direction of motion of the airplane is:

$$T_R - D - W \sin(\theta) \quad \text{in which} \quad D = \frac{1}{2} \rho_\infty S C_D V_\infty^2 \tag{4}$$

in which T_R is the thrust produced by the propulsion system and D is the drag.

2.1 Load factor

According to Eq. (3), the value of the load factor is

$$n = \frac{L}{W} = cos(\theta)$$

It is constant on the trajectory and in order to ensure the integrity of the airplane structure, its value has to be limited such that

$$n_{min} \leq n \leq n_{max},$$

Since n is always non-negative, this inequality implies that

$$cos(\theta) \leq n_{mx}$$

For most airplanes this condition is satisfied by the fact that $n_{max} > 1$.

2.2 Lift coefficient

Upon replacing L by its expression in Eq. (3), the following expression for the lift coefficient C_L is obtained:

$$C_L = \frac{2W\,cos(\theta)}{\rho_\infty S V_\infty^2} \tag{5}$$

Thus, C_L changes in time as W and ρ_∞ vary, but it must always satisfy the constraint

$$C_L \leq C_{Lmax} \tag{6}$$

We introduce the variable $\tilde{W}$, which encompasses all the time varying terms on the right-hand side of Eq. (5), as

$$\tilde{W} = \frac{W}{\rho_\infty} \tag{7}$$

The definition of this variable will prove worthwhile, as most formulas derived hereafter will take a simpler form when expressed in terms of $\tilde{W}$. This variable has an intriguing physical meaning: it is the volume of air that has the same weight as the airplane, at the altitude of the airplane. Because of this, it could be referred to as the "airplane relative volume". Note that $\tilde{W}$ has the absolute maximum value $\tilde{W}_{MAX} = \frac{W_0}{\rho_\infty(h_c)}$, where W_0 is the airplane maximum weight and h_c its service ceiling and the absolute minimum value $\tilde{W}_{MIN} = \frac{W_1}{\rho_\infty(0)}$, where W_1 is the airplane empty weight. We define $\tilde{W}_i = \tilde{W}(t_i)$ and $\tilde{W}_f = \tilde{W}_f(t_f)$. Given Eq. (5), Ineq. (6) can be written as

$$\tilde{W}(t) \leq \overline{C}_{Lmax} \;\forall\; t, \quad \text{with } \overline{C}_{Lmax} = \frac{S V_\infty^2 C_{Lmax}}{2\,cos(\theta)} \text{ a constant} \tag{8}$$

Ineq. (8) is satisfied at all times if and only if

$$\tilde{W}_{max} \leq \overline{C}_{Lmax} \tag{9}$$

where $\tilde{W}_{MAX}$ denotes the maximum value of $\tilde{W}$ on the trajectory. We will similarly denote by $\tilde{W}_{min}$ its minimum value. It will be crucial for the flyability analysis of trajectories to know the values of

$\tilde{W}_{min}$ and $\tilde{W}_{max}$. These are determined in Appendix B, together with some other important properties of $\tilde{W}$. In any case, a necessary condition for Ineq.(5) to hold is that it holds at $t = t_i$. This yields the following lower bound on the speed:

$$V_\infty \geq V_{LB} \quad \text{with} \qquad V_{LB}^2 = \frac{2\tilde{W}_i \cos(\theta)}{SC_{L\,max}} \tag{10}$$

2.3 Fuel consumption

The mass of the airplane changes as fuel is burned by its engines. Labonté (2012) discussed how to allow for this process in Newton's equation of motion and showed that it then becomes

$$-AFR\left[\frac{dM}{dt}\right]V_\infty = T_R - D - W\sin(\theta) \tag{11}$$

in which AFR is the Air to Fuel Ratio in the combustion engine. Since $P_R = V_\infty T_R$, Eq. (1) implies

$$T_R = -\frac{\eta}{cV_\infty}\left[\frac{dW}{dt}\right] \tag{12}$$

Therefore, Eq. (11) yields the following differential equation for the airplane weight W:

$$\frac{(AFR)V_\infty}{g}\left[\frac{dW}{dt}\right] = -\frac{\eta}{cV_\infty}\left[\frac{dW}{dt}\right] - D - W\sin(\theta) \tag{13}$$

Upon expressing C_D in terms of C_L and using for C_L the value given in Eq. (5), Eq.(13) becomes the Riccati equation:

$$G(V_\infty)\frac{dW}{dt} = -\rho_\infty Q(\tilde{W}) \qquad \text{with} \qquad Q(\tilde{W}) = \alpha + \beta\tilde{W} + \delta\tilde{W}^2 \tag{14}$$

in which α, β, δ and G are the following constants:

$$\alpha = \alpha_1 V_\infty^2 \qquad \beta = \sin(\theta) \qquad \delta = \frac{\delta_1}{V_\infty^2}$$

And

$$\alpha_1 = \frac{S\,C_{D0}}{2} \qquad \delta_1 = \frac{2\cos^2(\theta)}{\pi\, e\, AR\, S} \qquad G(V_\infty) = \left[\frac{\eta(V_\infty)}{cV_\infty} - \frac{(AFR)V_\infty}{g}\right] \tag{15}$$

We note that the coefficient $G(V_\infty)$ of dW/dt depends only on the speed and has the same value whether the airplane is ascending or descending. When the airplane is non-descending, the constants α and δ are positive and β is non-negative; therefore $Q(\tilde{W}) > 0\ \forall \tilde{W}$. Therefore, G has to be positive otherwise, according to the differential equation, W would be increasing when the airplane is non-descending. Fig. 1 shows the graph of G as a function of V_∞ for the Cessna 182 and the Silver Fox-like UAV. For the latter airplane, this condition on the coefficient results in the existence of an upper bound V_{UB0} on V_∞, due to the fact that the propeller efficiency goes to zero and becomes negative after a certain speed. For that airplane, $V_{UB0} = 66.0$ *m/s*. This bound depends

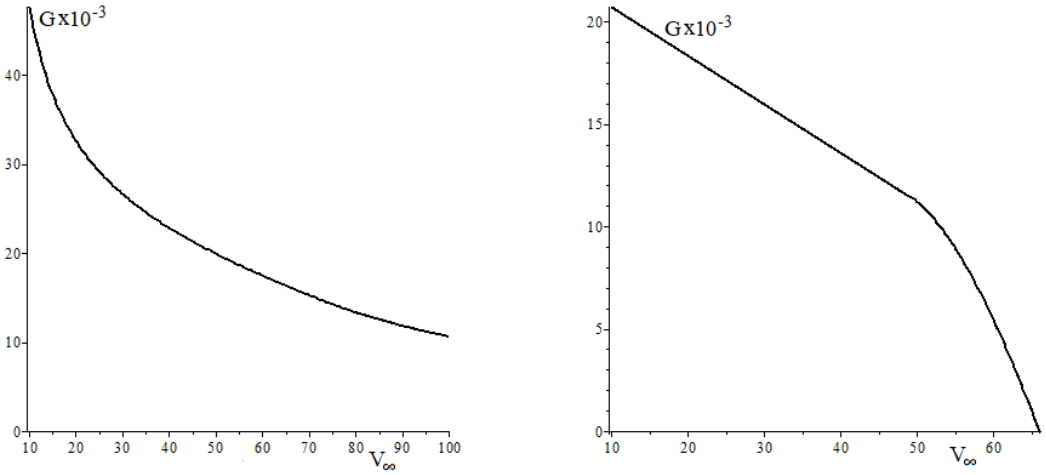

(a) Cessna 182 (b) Silver Fox-like UAV

Fig. 1 Graph of $G(V_\infty)$, the coefficient of dW/dt in terms of V_∞

only on the characteristics of the airplane: It has the same value for all trajectories. When the airplane is descending, $\beta < 0$; constraints will have to be imposed so that

$$Q(\tilde{W}) \geq 0 \tag{16}$$

since otherwise, according to Eq. (14), the weight of the airplane would increase, which is not possible. We shall examine, in the following sections, the conditions that must be imposed on θ and V_∞ for Ineq. (16) to be satisfied. Note that whatever the trajectory considered, it is necessary that there be enough fuel to fly it; this yields the condition

$$W(t_f) \geq W_1$$

Upon assuming that the above mentioned conditions are satisfied, Eq. (14) can be exactly solved, as described in Labonté (2012); its solution being a combination of confluent hypergeometric functions. However, we are not obliged to use the solution in this form because Labonté (2015) has shown that a one-step Runge-Kutta approximation of order four produces essentially the exact value of $W(t)$. It is then this expression for the solution that we shall use. Accordingly, the weight of the airplane is given by $W(t)$:

$$W(t) = W_i + \frac{1}{6}\left[A(t) + 2B(t) + 2C(t) + D(t)\right] \tag{17}$$

in which

$$A(t) = \Delta t\, F(t_i, W_i), \qquad B(t) = \Delta t\, F(t_m, W_i + A(t)/2)$$
$$C(t) = \Delta t\, F(t_m, W_i + B(t)/2) \qquad D(t) = \Delta t\, F(t, W_i + C(t))$$

$$F(t,W) = -\frac{1}{G(V_\infty)}\left[\alpha\rho_\infty + \beta W + \delta\rho_\infty^{-1}W^2\right] \qquad \Delta t = t - t_i, \quad t_m = t_i + \Delta t/2$$

Fig. 2 shows how W and $\tilde{W}$ vary with time, as the Silver Fox-like UAV, ascends on a rectilinear

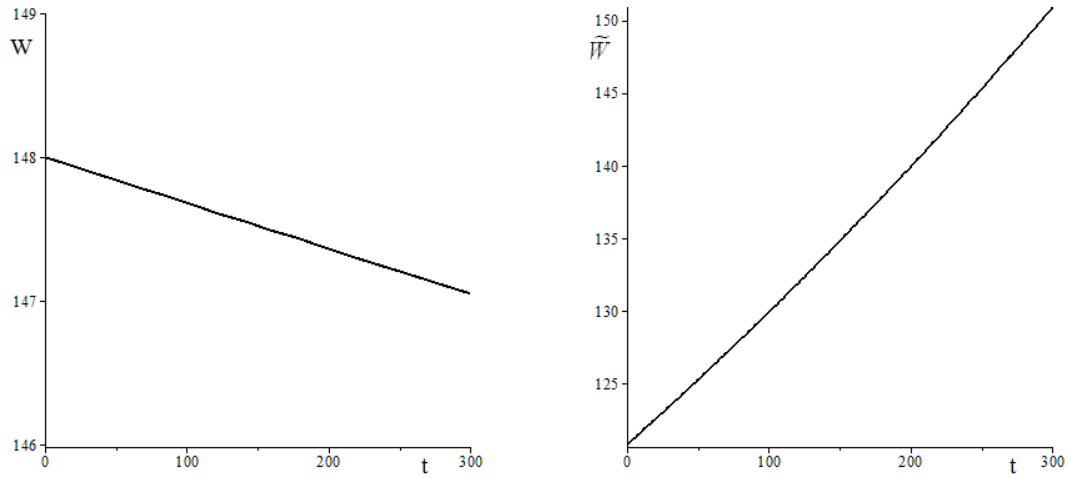

(a) Weight *W(t)* (b) Relative volume $\tilde{W}(t)$

Fig. 2 Weight variation in time for a Silver Fox-like UAV ascending with $\theta = 15°$ and $V_\infty = 30$ *m/s*

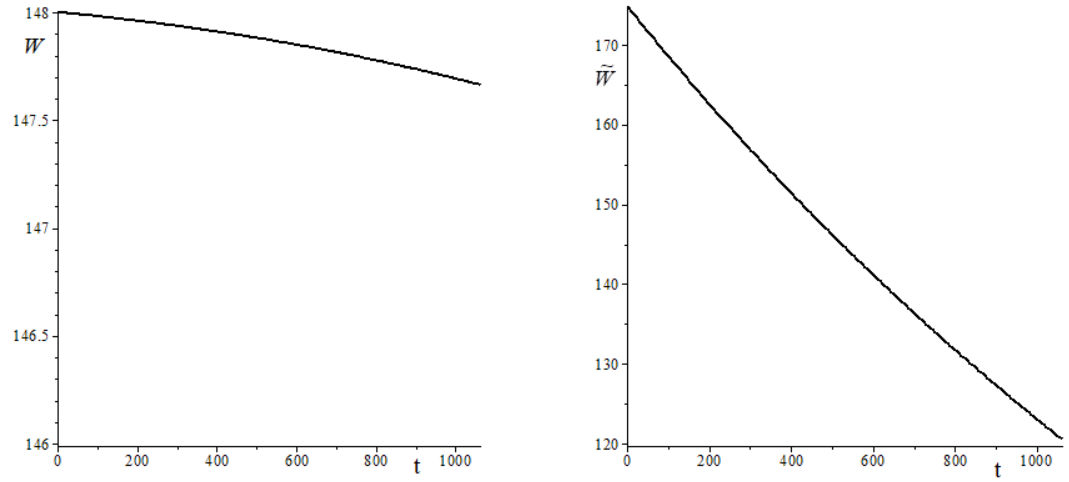

(a) Weight *W(t)* (b) Relative volume $\tilde{W}(t)$

Fig. 3 Weight variation in time for a Silver Fox-like UAV descending with $\theta = -5°$ and $V_\infty = 40$ *m/s*

trajectory inclined at *15°* and speed $V_\infty = 30$ *m/s*, during *300* s. It is to be remarked that *W* is nearly a linear function of time; thus the linear approximation for *W(t)*, discussed in Labonté (2015) could also very well be used instead of the solution given by Eq. (17). Fig. 3 shows similar graphs as in Fig. 2, for a descending trajectory inclined at *-5°* with a speed of *40* m/s.

3. Constraints related to the power

We note that according to Eqs. (1) and (14), the power required for the motion is

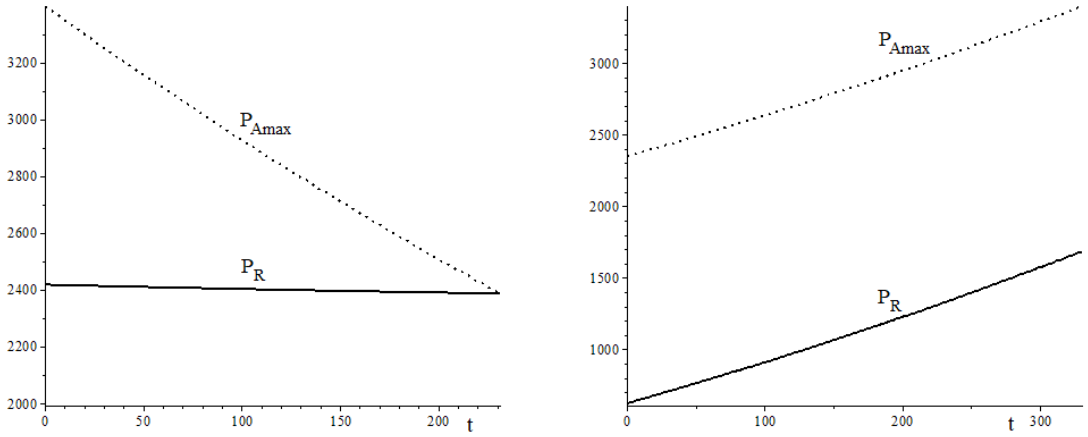

(a) Ascending with θ = 50°, V_∞ = 20.0 m/s (b) Descending with θ = -5°, V_∞ = 64.5 m/s

Fig. 4 Power required P_R and maximum power available P_{Amax} for the Silver Fox-like UAV

$$P_R = \frac{\eta \rho_\infty}{cG} Q(\tilde{W})$$

Thus, the non-negativity of Q corresponds to the non-negativity of P_R. It is necessary that the airplane propelling system be able to provide enough power for the motion to be possible. Thus, it is required that

$$P_R \le P_{Amax} \quad \text{i.e.,} \quad Q(\tilde{W}) \le \frac{cG\,P_{P\,max}(0)}{\rho_s} \tag{18}$$

where P_{Amax} is the maximum power available for the motion. Fig. 4(a) shows how P_R and P_{Amax} vary in time when the Silver Fox-like UAV ascends at *50°*, with V_∞ = *20.0* m/s. Fig. 4(b) shows the same parameters when the Silver Fox-like UAV descends at *-10°*, with V_∞ = *64.5* m/s.

3.1 Non-negativity of the power for descending trajectories

In this section, we examine the conditions under which Ineq. (16) is satisfied. As a function of $\tilde{W}$, Q corresponds to an upward concave parabola with minimum at $\tilde{W}_c$:

$$\tilde{W}_c = -\frac{\beta}{2\delta} \tag{19}$$

This point lies on the positive $\tilde{W}$-axis since β is negative and at that point,

$$Q(\tilde{W}_c) = \alpha - \frac{\beta^2}{4\delta} = -\frac{\Delta}{4\delta}$$

where Δ is the discriminant of Q:

$$\Delta = sin^2(\theta) - \frac{4C_{D0}}{\pi\, eAR} cos^2(\theta) \tag{20}$$

We note that what is normally considered as the gliding angle θ_g is the angle at which the power required P_R is null, i.e. the angle at which $Q = 0$, this angle would therefore be

$$\theta_g = -tan^{-1}\left[\frac{4C_{D0}}{\pi eAR}\right]$$

It should be remarked however that there are actually no constant values of θ and V_∞ for which P_R remains null on the whole trajectory. Indeed, $\tilde{W}$ changes as the air density varies with the altitude and therefore it cannot remain at the value $\tilde{W}_c$. We discuss gliding further in Section 12.3.

If $\Delta \leq 0$, i.e. the trajectory is not more inclined than θ_g, then Q does not have real roots or has a double real root and therefore Ineq. (16) is satisfied at all times. On the other hand, if $\Delta > 0$, $Q(\tilde{W})$ has two positive real roots r_- and r_+

$$r_\pm = \frac{1}{2\delta}\left[-\beta \pm \sqrt{\Delta}\right] = V_\infty^2 r_{0\pm} \tag{21}$$

Note that Δ is independent of the speed V_∞ while $r_\pm$ have an overall factor of V_∞^2, which is made explicit in Eq. (21) where $r_{0\pm}$ are independent of V_∞. The inequality $Q \geq 0$ is satisfied when one of the two following inequalities is satisfied

$$\tilde{W} \leq r_- \tag{22}$$

or

$$\tilde{W} \geq r_+ \tag{23}$$

Because the two roots r_- and r_+ are separated, while $\tilde{W}$ is continuous, $\tilde{W}$ must always remain in the same one of the two intervals defined by Ineqs. (22) and (23).

3.1.1 The braking forces

Note that in all cases, Ineq. (16) must be satisfied at $t = t_i$; this condition can be written as:

$$\alpha_1 V_\infty^4 + \left(\beta \tilde{W}_i\right) V_\infty^2 + \left(\delta_1 \tilde{W}_i^2\right) \geq 0$$

The left-hand side of this inequality is a quadratic function of V_∞^2, which corresponds to an upward concave parabola. This function may or may not have roots, depending on the value of its discriminant, which is $\Delta \tilde{W}_i^2$, with Δ given in Eq. (20). If it has roots, these are simply

$$V_\pm^2 = \tilde{W}_i\, r_{0\pm}$$

the factors $r_{0\pm}$ being the same as in Eq. (21). Fig. 5 shows how $Q(\tilde{W}_i)$ varies in term of the speed V_∞ for the Cessna 182, when $\theta = -5°$.

As can be seen in Eqs. (3) and (4), the lift cancels the component of gravity that is perpendicular to the velocity and the drag opposes the component of gravity along the velocity. Thus, the drag must be strong enough to cancel enough of the force of gravity for the speed to remain constant. It is interesting to note that the two separate domains $V_\infty \leq V_-$ and $V_\infty \geq V_+$ correspond respectively to the separate regions in which it is the lift induced drag and the parasite drag that dominates the force of gravity. In Fig. 6 the full line and the dotted line represent respectively the lift induced drag and the parasite drag, for the Cessna 182 on a trajectory with $\theta =$

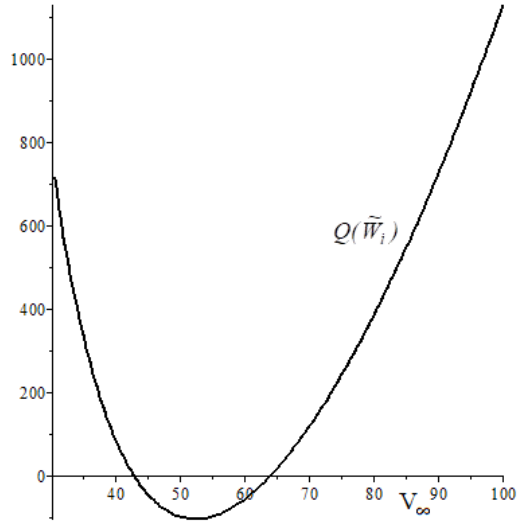

Fig. 5 Graph of $Q(\tilde{W}_i)$ as a function of V_∞ for the Cessna 182, when θ = -5°

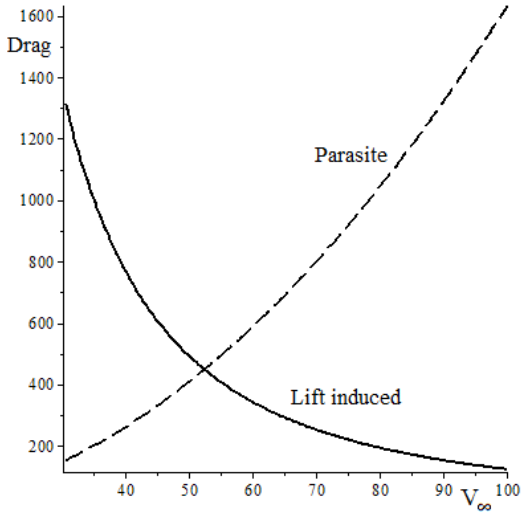

Fig. 6 Graphs of the lift induced drag (full line) and parasite drag (dotted line) for the Cessna 182

–5°. These forces dominate respectively at low and large speeds. However, this ceases to be the case in the interval (V_-, V_+), in which the airplane would therefore accelerate.

3.2 Sufficiency of the power

The airplane propelling system should be able to provide enough power for its motion on the trajectory to be possible. Thus, it is required that Ineq. (18) hold, that is

$$Q_A(\tilde{W}) \le 0 \quad \text{with} \quad Q_A(\tilde{W}) = \overline{\alpha} + \beta\tilde{W} + \delta\tilde{W}^2 \tag{24}$$

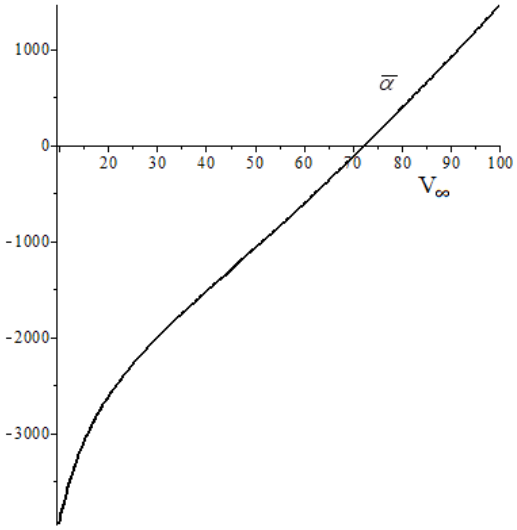

Fig. 7 Graph of $\overline{\alpha}$ as function of V_∞, for the Cessna 182

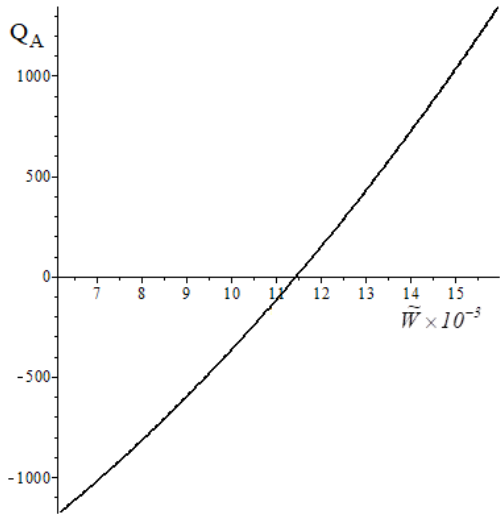

Fig. 8 Q_A for the Cessna 182 with $V_\infty = 30$ m/s and $\theta = 5°$

in which

$$\overline{\alpha} = \alpha - \frac{c\,GP_{P\,max}(0)}{\rho_s}$$

The parameter $\overline{\alpha}$, as α itself, depends only on the speed V_∞ and has the same value for ascending and non-ascending trajectories. Fig. 7 shows how $\overline{\alpha}$ varies with V_∞, for the Cessna 182; its behavior for the Silver Fox-like UAV is very similar. Note that it is necessary to have a mathematical representation for $\eta(V_\infty)$ in order to analyze Ineq. (24). The function Q_A corresponds to the same upward concave parabola as Q, except that it is translated downward by the constant

$cGP_{Pmax}(0) / \rho_s$. Its minimum occurs at the position $\tilde{W}_c$. It is necessary that the discriminant Δ_A of Q_A be positive in order for Q_A to have two separate real roots, and that there be a non-trivial interval in which Q_A is non-positive. Its two real roots are

$$r_{A\pm} = \frac{1}{2\delta}\left[-\beta \pm \sqrt{\Delta_A}\right] \tag{25}$$

These two roots $r_{A\pm}$ depend on θ and V_∞ but are independent of t. For all trajectories, it is necessary that

$$r_{A-} \le \tilde{W}(t) \le r_{A+} \ \forall t \tag{26}$$

4. Feasible ascending trajectories

For ascending trajectories, $\tilde{W}_c$, the position of the minimum of Q_A, is negative. It is therefore necessary that the intercept of Q_A on the ordinate axis be negative for Ineq. (24) to be possible when $\tilde{W} > 0$. This means that $\overline{\alpha} < 0$, which implies an upper bound V_{UB2} on V_∞:

$$V_\infty < V_{UB2} \tag{27}$$

For the Cessna 182, $V_{UB2} = 72.39$ m/s and for the Silver Fox-like UAV, $V_{UB2} = 56.35$ m/s. Because $\overline{\alpha} < 0$, the discriminant Δ_A of Q_A is always positive and, thus, Q_A has two real roots. The root r_{A-} is always negative and r_{A+} positive, Ineq. (24) is therefore satisfied if and only if

$$\tilde{W}(t) \le r_{A+} \ \forall \ t \tag{28}$$

Fig. 8 shows how Q_A varies as a function of $\tilde{W}$ for the Cessna 182 with $V_\infty = 30$ m/s and $\theta = 5°$. Ineq. (8) is of the same nature as Ineq. (28); and it can therefore be dealt with in the same manner.

We now consider the problem of determining if an airplane of initial weight W_i can fly on a trajectory with a given angle of inclination θ and, if so, for how long it can fly on this trajectory. The condition to satisfy is Ineq. (28). This inequality must obviously hold at $t = t_i$; this will be the case if the speed V_∞ is bounded above by V_{UB1}. It is then important to know if $\tilde{W}(t)$ is increasing or decreasing. According to the discussion done in Appendix B, $\tilde{W}(t)$ is monotonically increasing $\forall t > t_i$ if $\overline{Q}(\tilde{W}_i) \ge 0$ and if $\overline{Q}(\tilde{W}_i) < 0$, $\tilde{W}(t)$ will be decreasing for some time and then possibly reach a minimum value and increase afterwards. It is worth remarking that $\tilde{W}(t)$ is actually monotonically increasing except for very small inclination angles. The following two cases should be considered.

Case 1: $\overline{Q}(\tilde{W}_i) \ge 0$

It is then required that $\tilde{W}_i < r_{A+}$. An upper bound on the duration of the trajectory is then given by the time t_{end} at which $\tilde{W}(t)$ increases to the value r_{A+}, that is until

$$\tilde{W}(t_{end}) = r_{A+} \tag{29}$$

Case 2: $\overline{Q}(\tilde{W}_i) < 0$

In that case, $\tilde{W}(t)$ will be decreasing for some time so that Ineq. (28) will be satisfied until the end of the trajectory or the instant of time t_{end} at which Eq. (29) holds. Thus, the trajectory will last longer, the farther $\tilde{W}(t_i)$ is from r_{A+}. As can be seen in Fig. 9(a), the lower the speed, the farther r_{A+} will be from $\tilde{W}(t_i)$. Fig. 9(b) shows how $\tilde{W}(t)$ approaches r_{A+} as time goes on.

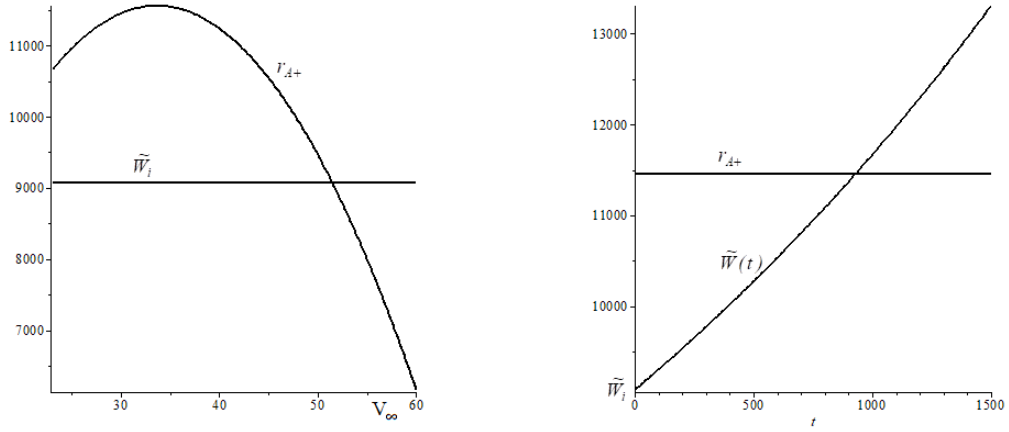

(a) r_{A+} and $\tilde{W}_i$ in terms of V_∞ (b) r_{A+} and $\tilde{W}(t)$ in terms of t

Fig. 9 Graphs for the Cessna 182, with $W_i = W_0$, $h_i = 0$ and $\theta = 5°$. (a) r_{A+} and $\tilde{W}_i$ as function of V_∞, (b) r_{A+} and $\tilde{W}(t)$ as functions of t, when the speed is *30* m/s

The condition that guarantees the sufficiency of the lift for the motion, expressed in Ineq. (8), can be treated the same way as described above, with r_{A+} replaced by $\bar{C}_{Lmax}$ in the above discussion. Note that the farther $\tilde{W}(t)$ starts from r_{A+}, the longer the trajectory will possibly be. Evidently, the trajectory terminates before t_{end} of Eq. (29) if the service ceiling is reached or the fuel is completely burned.

4.1 Example

Consider a Cessna 182 that starts at sea level with $W_i = W_0$, on a trajectory inclined at *5°*. Upon applying the procedure described above, one obtains

$$V_{LB} = 23.1 \text{ m/s}, \quad V_{UB1} = 51.4 \text{ m/s}, \quad V_{UB2} = 72.3 \text{ m/s},$$

we therefore consider the possible choice $V_\infty = 30$ *m/s*. The calculation of $\bar{Q}(\tilde{W}_i)$ yields the value *58,806.5* m^3, which is positive, thus indicating that $\tilde{W}(t)$ is monotonically increasing. The time required for the airplane to reach its service ceiling is calculated to be $t_c = 2{,}110.0$ s. The time t_+ at which Eq. (29) is satisfied is found to be *926.9* s. This is therefore the last instant at which the trajectory is flyable; the altitude reached at this time is *2,423.5* m. It can also straightforwardly be checked that $\tilde{W}_f < \bar{C}_{Lmax}$.

5. Feasible non-ascending trajectories

For such trajectories, $\tilde{W}$ is a monotonically decreasing function of t, as pointed out in Appendix B. Therefore $\tilde{W}_{max} = \tilde{W}_i$ and $\tilde{W}_{min} = \tilde{W}_f$. Ineq. (8) is then satisfied if and only if the bound on V_{LB}, given in Eq. (10), is satisfied. $\tilde{W}$ must further satisfy Ineqs. (16) and (24). Fig. 10 shows the graphs of Q and Q_A as functions of $\tilde{W}$ for the Cessna 182 when $\theta = -5°$, for two different speeds.

We now show how to determine if an airplane of initial weight W_i can fly on a trajectory that starts at altitude h_i, with a given angle of inclination θ and, if so, how long it can fly on this trajectory. Recall that Ineqs. (16) and (24) must be satisfied at all times, thus, in particular at $t = t_i$:

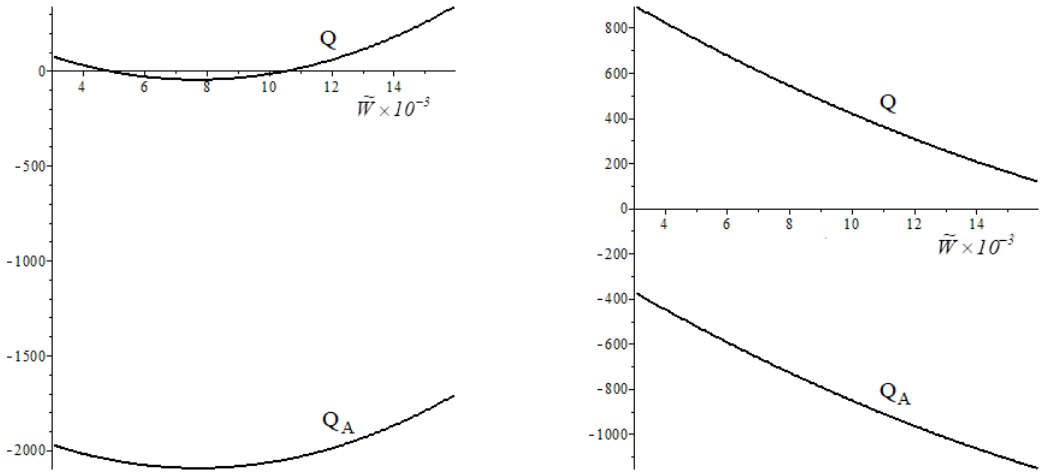

(a) $V_\infty = 35$ *m/s* (b) $V_\infty = 70$ *m/s*

Fig. 10 Graph of $\bar{Q}(\tilde{W})$ and $\bar{Q}_A(\tilde{W})$, for the Cessna 182, when $\theta = -5°$, for two different speeds V_∞

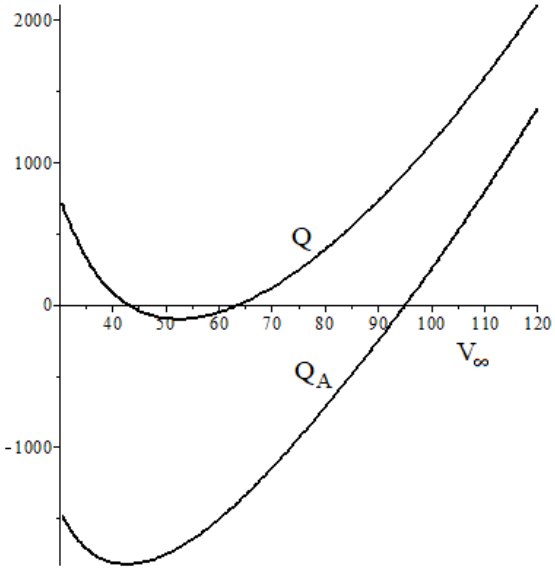

Fig. 11 Graph of Q and Q_A for the Cessna 182, at $t = t_i$ as functions of V_∞, when $\theta = -5°$

$$Q(\tilde{W}_i) \geq 0 \quad \text{and} \quad Q_A(\tilde{W}_i) \leq 0 \tag{30}$$

These inequalities impose restrictions on the possible values of V_∞. Fig. 11 show the graph of Q and Q_A for the Cessna 182, at $t = t_i$ as functions of V_∞, when $\theta = -5°$. In that case there are two disjoint domains of possible speeds. The speed has to be selected so that Ineqs. (30) are satisfied. The following two cases have to be considered.

Case 1: The roots $r_\pm$ are complex or they are real with $\tilde{W}_i \leq r_-$. The maximum duration of the trajectory is determined by the instant t_{end} at which

$$\tilde{W}(t_{end}) = r_{A-} \tag{31}$$

Case 2: The roots $r_{\pm}$ are real with $\tilde{W}_i > r_+$. Note that $\tilde{W}_i$ has to be actually greater than r_+, otherwise the trajectory would consist in a single point because the maximum duration of the trajectory is determined by the instant t_{end} at which

$$\tilde{W}(t_{end}) = r_+ \tag{32}$$

Evidently, the trajectory terminates before t_{end} of Eq. (31) or (32) if the sea level is reached or the fuel is completely burned.

5.1 Example

Consider the Cessna 182 that starts at its service ceiling with $W_i = W_0$, on a trajectory inclined at *-5*°. Eq. (10) yields $V_{LB1} = 30.6$ m/s. Ineqs. (30) yield the two possible ranges for the speed

$$[V_{LB1}, 42.9] \text{ m/s} \quad \text{and} \quad [64.0, 95.2] \text{ m/s} \tag{33}$$

Let us consider the speed $V_\infty = 35$ m/s, which is in the first of these intervals. With this speed, Ineqs. (30) are satisfied. $\tilde{W}_i > r_+$ and the maximum duration of the trajectory is until t_{end} given by Eq. (32), thus $t_{end} = 1{,}281.1$ s. The final altitude reached is then *1,609.1* m. Upon considering the speed $V_\infty = 70$ m/s, which is in the second interval, one finds that Ineqs. (30) are satisfied and $\tilde{W}_i \leq r_-$. Eq. (31) yields $t_{end} = 1{,}281.3$ s and the final altitude reached is *1608.5* m.

6. Tables of flyability parameters

For the process of automatic trajectory construction, it can be very useful to dispose of tables that quickly help determine what angles of inclination and what speeds correspond to flyable trajectories. The analysis presented in this document, allow for the straightforward construction of such tables and we give examples of such tables below for the Cessna 182 and the Silver Fox-like UAV. In these tables, all the trajectories considered start with the largest possible weight $W_i = W_0$. The first line of the tables contains the value of θ, the second line contains the smallest possible speed V_m, the third line: the final altitude attainable at this speed. The forth line contains the largest possible speed V_M and the fifth line, the final altitude attainable at that speed. Only trajectories longer than *20* m are retained. Trajectories are flyable at all the speeds between V_m and V_M and their final altitude can be very different than those obtained with these two extreme speeds, which are at the edge of flyability. We recall that the service ceiling for the Cessna 182 is $h_c = 5{,}517$ m and for the Silver Fox-like UAV, it is $h_c = 3{,}700$ m. For ascending trajectories, the initial altitude is *0* and for descending trajectories, it is h_c. Note that the bounds on the speeds have not been determined with great precision; our intention in producing these table was mainly to give an idea of the possible ranges of parameters for flyable trajectories.

6.1 Ascending trajectories

Section 4 provides the necessary information for the construction of the tables. Accordingly, an inclination angle is selected and then the flyability of trajectories is tested with different values of the speed. All inclination angles, by increments of 2.5° for the Cessna and by 5° for the Silver Fox-like UAV, are considered until angles, for which no flyable trajectories are reached.

Table 1 Flyable trajectories for the Cessna 182

θ	2.5	5	7.5
V_m	23.2	23.2	23.1
h_{max}	80.6	109.6	67.2
V_M	61.0	51.0	39.4
h_{max}	188.6	145.8	26.2

Table 2 Flyable trajectories for the Silver Fox-like UAV

θ	5	10	20	30
V_m	15.8	15.7	15.5	14.8
h_{max}	39.8	25.9	256.6	139.1
V_M	52.7	47.8	35.7	21.0
h_{max}	299.0	249.8	52.5	46.2

Table 3 Flyable trajectories for the Cessna 182

θ	0	-2.5	-5		-7.5	-10
V_m	30.7	30.7	30.7	64.0	89.2	105.7
h_{min}	h_c	0	0	0	0	1668.0
V_M	63.5	80.6	42.7	95.0	108.0	119.7
h_{min}	H_c	5427.0	5426.6	5417.6	5440.9	5425.5

Table 4 Flyable trajectories for the Silver Fox-like UAV

θ	0	-2.5	-5	-10	-12.5
V_m	19.0	19.0	35.1	54.9	61.8
h_{min}	h_c	0	0	0	0
V_M	55.9	58.0	59.9	63.4	64.8
h_{min}	h_c	3166.4	3410.8	3642.2	3426.58

6.2 Non-ascending trajectories

Section 5 contains the necessary information for the construction of the tables. The method is the same as described above for the ascending trajectories.

6.3 Remarks on gliding

Gliding is considered to play an important role in the landing of airplanes. It allows airplanes to remain longer at high altitudes and spend less time at lower altitudes. Since the motor is at minimum power, the noise is minimized, and fuel consumption is also minimized see, for example, the discussion in Cunningham (1977), Dejarnette (1984), Clarke *et al*. (2013). The treatment of gliding flight that is found in most airplane dynamics books (for example, in Section 2.6 of Stengel (2004), Section 3.5 of Yechout *et al*. (2003), Section 12.7 of Houghton and Carruthers (1982), Section 6.9 of Anderson (2000), Section XI§3 of Cowley and Levy (1920)) is as follows.

The power required is set to zero in Eq. (4) so that there would be no fuel used. Both the angle

of the trajectory and the speed V_∞ are considered constant. It then follows that

$$D = -mg\sin(\theta_g)$$

Together with Eq (3), this yields

$$\tan(\theta_g) = -\left[\frac{C_{D0}}{C_L} + \frac{C_L}{\pi eAR}\right] \tag{34}$$

The maximum horizontal distance occurs when θ_g is minimum, which is when

$$C_{Lg} = \sqrt{\pi eARC_{D0}}\ ,$$

at which point

$$\tan(\theta_g) = -2\sqrt{\frac{C_{D0}}{\pi eAR}}$$

The gliding speed is obtained from the expression for the lift L, given in Eq. (3), in which the value of the lift coefficient C_{Lg} is entered. This yields

$$V_g = \sqrt{\frac{2W}{\rho_\infty S}}\left\{C_{D0}[4C_{D0} + \pi eAR]\right\}^{-1/4} \tag{35}$$

It should be noted that, as is evident from our discussion of descending trajectories, there are in fact no constant values of θ and V_∞ for which the power required P_R is null on the whole trajectory. As seen in Section 8, there is only one value of $\tilde{W}$ at which P_R is null: it is the constant value $\tilde{W}_c$ but $\tilde{W}$ never remains at this value; it necessarily changes on the trajectory, due to the variation of the air density as the airplane descends.

For the Cessna 182, Eq. (34) yields $\theta_g = -0.0808$ radians or *-4.628°*. Eq. (35) yields different values for V_g, according to the altitude at which it is evaluated, because of the parameter ρ_∞ that it contains: at the service ceiling, $V_g = 52.4$ m/s and at the sea level $V_g = 20.7$ m/s. Note that, as seen in Section 8, the bound on the lift coefficient implies the lower bound V_{LBI} on the speed, with $V_{LBI} = 30.6$ m/s for the Cessna 182. The following tables show the amount of fuel used in the descent at θ_g at various speeds. In these tables t_f is in minutes and ΔW is in Newtons. It covers the speeds from V_{LBI} to *70* m/s.

As Table 5 shows, the smallest amount of fuel is used at about *50* m/s. We performed further calculations in order to determine the speed that would require less fuel. The results obtained are shown in Table 6.

Table 6 indicates that the optimal speed for fuel usage is $V_\infty = 45.0$ m/s, at which point only *0.87* N of fuel is required, which is about *115* ml of fuel. Note that at the speed $V_g = 52.4$ m/s, calculated at h_c, the amount of fuel used is still only about *450* ml. It is therefore not a very costly approximation to consider this speed as the gliding speed.

For the Silver Fox-like UAV, Eq. (34) yields $\theta_g = -0.0729$ radians or *-4.174°*. Eq. (35) then yields $V_g = 77.1$ m/s at the service ceiling and $V_g = 64.1$ m/s at the sea level. However, the maximum allowed speed on such a descending trajectory is *59.3* m/s, which is at the bottom of the

Table 5 Time of flight and fuel used for the Cessna 182 at various speeds

$\theta = -4.628°$						
V_∞	30.7	40	50	52.4	60	70
t_f	37.12	28.49	22.79	21.75	18.99	16.28
ΔW	25.64	3.08	2.01	3.38	10.32	24.13

Table 6 Time of flight and fuel used at speeds close to the minimal fuel speed

$\theta = -4.628°$					
V_∞	40	45	46	47	48
t_f	25.90	25.32	24.77	24.25	23.74
ΔW	0.99	0.87	0.88	1.00	1.24

Table 7 Time of flight and fuel used for the Silver Fox-like UAV at various speeds

$\theta = -4.174°$					
V_∞	19.0	25	30	40	59.3
t_f	44.59	33.89	28.24	21.18	14.29
ΔW	0.15	0.02	0.15	0.65	3.56

gliding speeds range. Table 7 shows the time of flight and the amount of fuel used when descending from h_c to sea level at various speeds.

As Table 7 indicates, descending at the supposedly optimal fuel speed of *59.3* m/s, *3.56* N of fuel are required. This is an appreciable amount of fuel (19%), given the fact that the Silver Fox-like UAV has a maximum of *19.1* N of fuel. As can be seen in this table, the optimal fuel economy is actually obtained when descending at *25.0* m/s.

In concluding section, we make the following remarks about gliding.

1. There are actually no constant values of θ and V_∞ for which the power required P_R is null on the whole trajectory.
2. The formula normally used for the gliding speed is inaccurate in that the value it yields depends on the altitude at which it is evaluated.
3. The actual speed at which the consumption of fuel is minimum may be far from the speeds given by the gliding speed formula. It can be straightforwardly be determined by the trajectory analysis method developed in the previous sections.

7. Conclusions

The main contribution of this study is a method for determining all the constraints on the trajectories that are imposed by the dynamical abilities of an airplane. This constitutes a very important result as it provides information that is essential for automatic airplane trajectory planning. Another important contribution is the presentation of an approach for extracting meaningful information from these constraints, which is far from trivial, given that they correspond to inequalities with many variables.

General formulas are provided that express the necessary and sufficient conditions for an airplane to be able to follow a specified ascending or descending rectilinear trajectory at constant

velocity. These formulas yield the possible angles of inclination of flyable trajectories, the minimum and maximum speeds that the airplane can have, the fuel it requires, the time it requires to fly it and the maximum altitude difference between the starting and the finishing points. We believe that most of these formulas are original, in that they have never been published before. They are absolutely crucial for providing autonomy to fixed-wings drones. They also constitute, an important tool for the analysis of general airplane performances.

An intriguing new concept stood out, in that the variable $\tilde{W} = W / \rho_\infty$ plays a crucial role in all the formulas derived. Intriguingly, this variable corresponds to the volume of air that has the same weight as the airplane; we thus referred to it as the "airplane relative volume". It could be worthwhile exploring the particular significance of that variable, some important properties of which are exhibited in Appendix B.

In Sections 11 and 12, we have shown examples of tables of parameters for which trajectories are flyable, for both the Cessna 182 and a Silver Fox-like UAV. It is seen, in those tables that the ranges of possible speeds become smaller as the trajectories become steeper. The most remarkable fact however is that much less inclined descending trajectories are flyable at constant velocity than ascending trajectories. This is due to the fact that when the airplane is descending, the force of gravity tends to accelerate its fall, while it has no other mean that its drag to balance this force. Some original remarks are made about gliding, which is a particularly important mode of descent. These include the facts that rigorous gliding cannot be done at constant speed on a rectilinear trajectory and that the gliding speed formula is inaccurate. It is a worthwhile side benefit of the present work to straightforwardly allow determining the speed of minimum fuel use.

Such tables, as those shown as examples, could easily be stored in a small memory on-board the airplane, from which their information could be read when the need arises. This approach would be appropriate for automatic trajectory planners even for airplanes endowed with only small microcontrollers.

References

Airliners.net (2015), Cessba 182 Skylane; Airliners.net, Santa Monica, CA, U.S.A. www.airliners.net/aircraft-data/stats.main?id=145.

Allaire, F., Tarbouchi, M. and Labonté, G. (2009), "FPGA implementation of genetic algorithm for UAV real-time path panning", *J. Intel. Robot. Syst.*, **54**(1-3), 495-510.

Ambrosino, G., Ariola, M., Ciniglio, U., Corraro, F., De Lellis, E. and Pironti, A. (2009), "Path generation and tracking in 3-D for UAVs", *IEEE Trans. Control Syst. Technol.*, **17**(4), 980-988.

Anderson, J.D. Jr. (2000), *Introduction to Flight*, 4th Ed., McGraw-Hill Series in Aeronautical and Aerospace Engineering, Toronto, Ontario, Canada.

Askari, A., Mortazavi, M. and Talebi. H.A. (2015), "A new approach in UAV path planning using Bezier–Dubins continuous curvature path", *Proceedings of the Institution of Mechanical Engineers*, *Part G: Journal of Aerospace Engineering*, **230**(6), 1103-1113.

Babaei, A.R. and Mortazavi, M. (2010), "Three-dimensional curvature-constrained trajectory planning based on in-flight waypoints", *J. Aircraft*, **47**(4), 1391-1398.

Carpenter, P. (2018), "RC aerobatic airplanes", RC Airplane World, www.rc-airplane-world.com/rc-aerobatic-airplanes.html.

Cavcar, M. (2004), "Propeller", School of Civil Aviation, Eskisehir, Turkey, https://fr.scribd.com/document/230664341/Propeller.

Chandler, P., Rasmussen, S. and Pachter, M. (2000), "UAV cooperative path planning", *Proceedings of the AIAA Guidance*, *Navigation*, *and Control Conference*, Denver, Colorado, U.S.A, August.

Chitsaz, H. and LaValle, S.M. (2007), "Time-optimal paths for a Dubins airplane", *Proceedings of the 46th IEEE Conference on Decision and Control*, New Orleans, Luisiana, U.S.A., December.

Commercial Aviation Safety Team (CAST) (2011), "Propeller operation and malfunctions basic familiarization for flight crews", CAST, www.cast-safety.org/pdf/4_propeller_fundamentals.pdf.

Cowley, W.L. and Levy, H. (1920), *Aeronautics in Theory and Experiment*, 2nd Ed., Edward Arnold Publisher, London, United Kingdom.

Cunningham, F.L. (1977), "The profile descent", *American Institute of Aeronautics and Astronautics (AIAA) Aircraft Systems & Technology Meeting*, Seattle, Washington, August 22-24.

Dejarnette, F. (1984), "Effects of aircraft and flight parameters on energy-efficient profile descents in time-based metered traffic", *Proceedings of American Institute of Aeronautics and Astronautics (AIAA)*, *17th Fluid Dynamics*, *Plasma Dynamics*, *and Lasers Conference*, *Fluid Dynamics and Co-located Conferences*, Snowmass, Colorado, U.S.A.

Dubins, L.E. (1957), "On curves of minimal length with a constraint on average curvature and with prescribed initial and terminal positions and tangents", *American J. Math.*, **79**, 497-516.

Eshelby, M.E. (2000), *Aircraft Performance: Theory and Practice*, American Institute of Aeronautics Inc., Reston, Virginia, U.S.A.

Filippone, A. (2006), *Flight Performance of Fixed and Rotary Wing Aircraft*, Butterworth-Heinemann, Burlington, MA, U.S.A.

Frazzoli, E., Dahleh, M.A. and Feron, E. (2005), "Maneuver-based motion planning for nonlinear systems with symmetries", *IEEE Trans*. *Robot*., **21**(6), 1077-1091.

Hale, F.J. (1984), *Introduction to Aircraft Performance*, *Selection*, *and Design*, John Wiley and Sons, New York, U.S.A.

Holub, J., Foo, J.L., Kilivarapu, V. and Winer, E. (2012), "Three dimensional multi-objective UAV path planning using digital pheromone particle swarm optimization", *53rd AIAA/ASME/ASCE/AHS/ASC Structures*, *Structural Dynamics and Materials Conference*, Honolulu, Hawaii, U.S.A., April.

Horizon Hobby (2017), GT80 Twin Cylinder (4.88 cu in); Horizon Hobby, www.horizonhobby.com/product/airplanes/airplane-accessories/airplane-engines-15042--1/gt80-twin-cylinder-(488-cu-in)-zene80t.

Hota, S and Ghose, D. (2010), "Optimal geometrical path in 3D with curvature constraint", *IEEE/RSJ International Conference on Intelligent Robots and Systems (IROS)*, Taipei, Taiwan, October.

Hota, S. and Ghose, D. (2014) "Optimal trajectory planning for path convergence in three-dimensional space", *J. Aerosp*. *Eng*., **228**(5), 766-780.

Houghton, E.L. and Carruthers, N.B. (1982), *Aerodynamics for Engineering Students*, 3rd Revised Ed., Edward Arnold Publisher, London, United Kingdom.

Hwangbo, M., Kuffner, J. and Kanade, T. (2007), "Efficient two-phase 3D motion planning for small fixed-wing UAVs", *IEEE International Conference on Robotics and Automation*, Rome, Italy, April.

Jia, D. and Vagners, J. (2004), "Parallel evolutionary algorithms for UAV path planning", *AIAA 1st Intelligent Systems Technical Conference*, Chicago, Illinois, September.

Jiabo, W., Li, L., Teng, L. and Zhu, W. (2012), "Three-Dimensional constrained UAV path planning using modified particle swarm optimization with digital pheromones", *EngOpt 2012 - 3rd International Conference on Engineering Optimization*, Rio de Janeiro, Brazil, July.

Judd, K.B. (2001), "Trajectory planning strategies for unmanned air vehicles", M.Sc. Dissertation, Brigham Young University, Provo, U.S.A.

Kamm, R.W. (2002), "Mixed up about fuel mixtures", Aviation Pros; www.aviationpros.com/article/10387634/mixed-up-about-fuel-mixtures.

Kok, K. Y. and Rajendran, P. (2016), "Differential evolution control parameter optimization for unmanned aerial vehicle path planning", *PLoS ONE*, **11**(3), e0150558.

Labonté, G. (2012), "Formulas for the fuel of climbing propeller driven planes", *Aircraft Eng*. *Aerosp*. *Technol*., **84**(1), 23-36.

Labonté, G. (2015), "Simple formulas for the fuel of climbing propeller driven airplanes", *Adv*. *Aircraft Spacecraft Sci*., **2**(4), 367-389.

Labonté, G. (2016), "Airplanes at constant speeds on inclined circular trajectories", *Adv. Aircraft Spacecraft Sci.*, **3**(4), 399-425

Lowry, J.T. (2011), "Propeller aircraft performance and the bootstrap approach", Aeronautics Learning Labratory for Science Technology and Research (ALLSTAR) of the Florida International University.

McIver, J. (2003), "Cessna Skyhawk II /100, performance assessment", Temporal Images, Melbourne, Australia. www.temporal.com.au/c172.pdf.

Neto, A.A., Macharet, D.G. and Campos, M.F.M. (2013), "Feasible path planning for vised-wing UAVs using seventh order Bésier curves", *J. Brazil. Comput. Society*, **19**(2), 193-203.

Niendorf, M., Schmitt, F. and Adolf, F.M. (2013), "Multi-query path planning for an unmanned vixed-wing aircraft", *AIAA Guidance*, *Navigation and Control (GNC) Conference*, Boston, MA, U.S.A., August.

Nikolos, I.K., Tsourveloudis, N.C. and Valavanis, K.P. (2003), "Evolutionary algorithm based 3-D path planner for UAV navigation", *IEEE Transactions on Systems*, *Man*, *and Cybernetics*, *Part B: Cybernetics*, **33**(6), 898-912.

Parsch, A. (2006), "Silver Fox", Directory of U.S. Military Rockets and Missiles, Appendix 4, www.designation-systems.net/dusrm/app4/silverfox.html.

Ramana, M.V., Varma, S.A. and Kothari, M. (2016), "Motion planning for a fixed-wing UAV in urban environments", *Conference Proceedings of the 4th IFAC Conference on Advances in Control and Optimization of Dynamical Systems ACODS 2016*, Tiruchirappalli, India, February.

Roberge, V., Tarbouchi, M. and Labonté, G (2012), "Comparison of parallel genetic algorithm and particle swarm optimization for real-time UAV path planning", *IEEE Trans. Industrial Inform.*, **9**(1), 132-141.

Roud, O. and Bruckert, D. (2006), *Cessna 182 Training Manual*, Red Sky Ventures and Memel CATS; Windhoek, Namibia. www.redskyventures.org.

Rudnick-Cohen, E., Azarm, S. and Herrmann, J.W. (2015), "Multi-objective design and path planning optimization of unmanned aerial vehicles (UAVs)", *16th AIAA/ISSMO Multidisciplinary Analysis and Optimization Conference*, Dallas, TX, U.S.A., June.

Stengel, R.F. (2004), *Flight Dynamics*, Princeton University Press, Princeton, New Jersey, U.S.A.

Torenbeek, E. (1976), *Synthesis of Subsonic Airplane Design*, Delft University Press, Rotterdam, Netherlands.

Wang, X., Jiang, P., Li, D. and Sun, T. (2017), "Curvature continuous and bounded path planning for fixed-wing UAVs", *Sensors*, **17**(9), 2155.

Wang, Z., Liu, L., Long, T., Yu, C. and Kou, J. (2014), "Enhanced sparse A* search for UAV path planning using dubins path estimation", *33rd Chinese Control Conference (CCC)*, Nanjing, China, July.

Weiwei, Z., Wei, W. Nengcheng, C. and Chao, W. (2014), "Efficient UAV path planning with multiconstraints in a 3D large battlefield environment", *Math. Problems Eng.*, **2014**.

Xia, L., Jun, X., Manyi, C., Ming, X. and Zhike, W. (2009), "Path planning for UAV based on improved A* algorithm", *9th International Conference on Electronic Measurement & Instruments*, *ICEMI '09*, Beijing, China, August.

Xian-Zhong, G., Zhong-Xi, H. Xiong-Feng, Z., Jun-Tao, Z. and Xiao-ian, C. (2013), "The shortest path planning for manoeuvres of UAV", *Acta Polytechnica Hungarica*, **10**(1), 221-239.

Yang, K. and Sukkarieh, S. (2010), "An analytical continuous-curvature path-smoothing algorithm", *IEEE Trans. Robot.*, **26**(3), 561-568.

Yechout, T.R., Morris, S.L., Bossert, D.E. and Hallgren, W.F. (2003), *Introduction to Aircraft Flight Mechanics: Performance*, *Static Stability*, *Dynamic Stability*, *and Classical Feedback Control*, American Institute of Aeronautics and Astronautics Inc., Reston, Virginia, U.S.A.

Zheng, C., Ding, M. and Zhou, C. (2003), "Real-Time route planning for unmanned air vehicle with an evolutionary algorithm", *J. Pattern Recogn. Artif. Intel.*, **17**(1), 63-81.

Appendix A: Reference airplanes

We note that there could be small differences between the values we list here and the actual values for a particular model of the airplanes considered. We used values that we could find on the internet or estimate from the values for similar airplanes. These data are quite adequate for our purpose that is to illustrate the calculations involved in the formulas we have derived.

The thrust of the Cessna 182 is provided by a reciprocating engine with constant speed propeller; that of the Silver Fox by a reciprocating engine with a fixed pitch propeller. We recall that the efficiency of the propeller is a function of the advance ratio J, defined as:

$$J = \frac{V_\infty}{N\,D}$$

in which N is its number of revolution per second and D is its diameter. Thus the maximum power available P_{Amax} will depend on the speed, according to the equation:

$$P_{Amax} = \eta(J) P_{max}$$

The dependence of η on J for a constant speed propeller has the general features shown in Fig. 12(a). This curve approximates that given in Cavcar (2004) by the following quadratic expressions:

$$\eta(J) = \left[\frac{0.663}{0.640}\right]\left[J - 0.8\right]^2 + 0.8 \qquad \forall J \le 0.8.$$

$$\eta(J) = 0.8 \qquad \forall J > 0.8.$$

The dependence of η on J for a fixed pitch propeller has the general features shown in Fig. 12(b). This curve approximates that given in the Aeronautics Learning Laboratory for Science Technology and Research (ALLSTAR) of the Florida International University (Lowry 2011) by the following quadratic expressions:

$$\eta(J) = -\left[\frac{0.83}{0.49}\right]\left[J - 0.70\right]^2 + 0.83 \qquad \forall J \le 0.7.$$

$$\eta(J) = -\left[\frac{0.83}{0.06}\right]\left[J - 0.70\right]^2 + 0.83 \qquad \forall J > 0.7.$$

Note that the propeller efficiency of this fixed pitch propellers goes to 0 at V_∞ = 66.1 m/s and becomes negative after that. Although a negative propeller efficiency might be desirable to slow down the airplane when it descends, it is not recommended to let this happens. When this happens, the propeller drives the engine and damage to the engine may result; see for example the Commercial Aviation Safety Team document (2011). We shall therefore not allow speeds larger than that value.

A.1 Cessna 182 Skylane

The parameters listed are W_1 = the weight of the empty airplane, W_0 = the maximum take-off

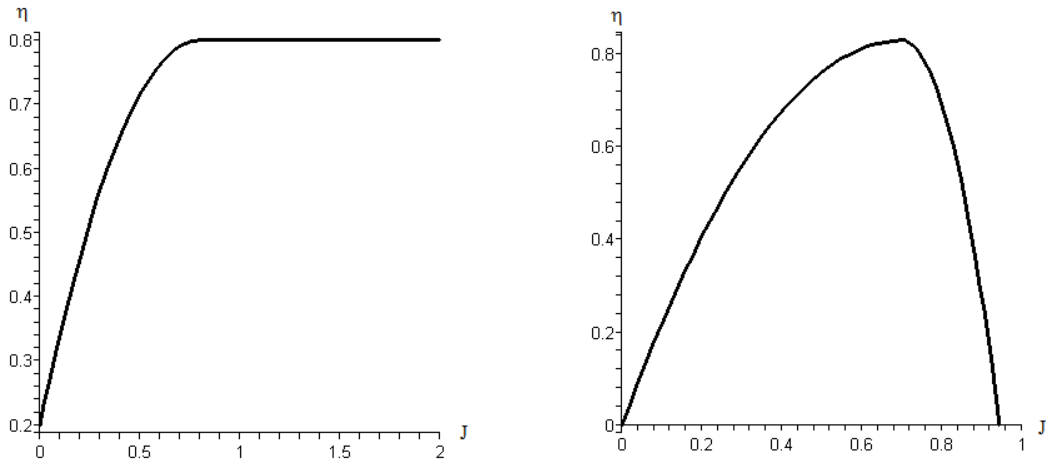

(a) Constant speed propeller (b) Constant pitch propeller

Fig. 12 Typical efficiency factor η as a function of the advance ratio J

Table 8 Characteristic parameters of the Cessna 182

W_1 = 7,562 N	W_0 = 11,121 N	W_F =1737 N
b = 11.02 m	S = 16.1653 m^2	e = 0.75
C_{Lmax} = 2.10	C_{D0} = 0.029	n_{max} = 3.8, n_{min} = -1.52
P_{Pmax} = 171.511 kW	RPM = 2,600	
Const. speed propeller	Diameter = 2.08 m	η_{max} = 0.80

weight, W_F = the maximum weight of fuel, b = the wingspan, S = the wing area, e = Oswald's efficiency factor, C_{Lmax} = the maximum global lift coefficient, C_{D0} = the global drag coefficient at zero lift, n_{max} and n_{min} are respectively the maximum and minimum value of the load factor, P_{Pmax} = maximum breaking power at sea level, RPM = number of revolution per minute, Diameter = diameter of the propeller, η_{max} = maximum value of the propeller efficiency.

The characteristic parameters for the Cessna 182 can be found in Airliners.net (2015), Roud and Bruckert (2006) and McIver (2003). Some of the parameters, which were not readily available, were estimated from those of the very similar Cessna 172.

A.2 Silver Fox-like UAV

The Silver Fox UAV is presently produced by Raytheon. Some of its specifications can be found at Parsch (2006). The power available $P_A(0)$ for the Silver Fox is only about 370 W, which allows it to climb only at low angles. Meanwhile, it is common for Radio Controlled (RC) airplanes to climb at very steep angles (See for example Carpenter (2018)). Thus, upon taking advantage of motors that have been developed in this domain, a Silver Fox-like airplane could be endowed with much more power in order to improve considerably its maneuver envelope. One such motor is the Zenoah GT-80 Twin Cylinder 80cc (ZENE80T). It weighs 34 N and outputs 4045 W at 7500 rpm. (Horizon Hobby 2017). We shall consider a Silver Fox-like UAV with such a motor.

Table 9 Characteristic parameters of the Silver Fox-Like airplane

W_1 = 100.0 N	W_0 = 148.0 N	W_F = 19.1 N
b = 2.4 m	S = 0.768 m^2	e = 0.8
C_{Lmax} = 1.26	C_{D0} = 0. 0251	n_{max} = 5.0, n_{min} = -2.0
P_{Pmax} = 4.413 kW	RPM = 7500	c = 7.4475×10^{-7}
Fixed pitch propeller	Diameter = 0.56 m	η_{max} = 0.77
h_c = 3700 m		

Appendix B: On the behavior of $\tilde{W}$

B.1 The behavior of $\tilde{W}$ for non-ascending trajectories

For non-ascending trajectories, $\theta \leq 0$ and $\tilde{W}$ is necessarily a monotonically decreasing function of time because W is monotonically decreasing and ρ_∞ is monotonically non-decreasing. Therefore, the maximum value of $\tilde{W}$ is $\tilde{W}_i$ and its minimum value is $\tilde{W}_f$.

B.2 The behavior of $\tilde{W}$ for ascending trajectories

For ascending trajectories, $\theta > 0$ and it is not evident whether $\tilde{W}$ is decreasing or increasing and what its maximum and minimum values are, because both the weight W and the air density ρ_∞ are monotonically decreasing functions of time. Since $\tilde{W}$ is continuous and differentiable, it reaches its maximum and minimum values at the two ends of the trajectory or, possibly at some intermediate critical points, where its derivative is null.

We shall hereafter prove that there is no such intermediate critical point at which $\tilde{W}$ is maximum and we shall also show that it is possible, for certain trajectories, for $\tilde{W}$ to have a local minimum at some intermediate point and that there would then be only one such intermediate minimum.

In order to determine if critical points exist, we obtain an equation for $\tilde{W}'(t)$. Given Eq. (14) and the fact that

$$\frac{d\rho_\infty}{dt} = -4.2433a_1 \sin(\theta)\frac{V_\infty \rho_\infty}{T(h)} \tag{36}$$

there follows the equation:

$$\frac{d\tilde{W}}{dt} = \frac{1}{G(V_\infty)}\overline{Q} \quad \text{with} \quad \overline{Q} = -\alpha - \overline{\beta}\tilde{W} - \delta\tilde{W}^2 \tag{37}$$

in which

$$\overline{\beta} = \overline{\beta}_1(t)\sin(\theta) \quad \text{with} \quad \overline{\beta}_1(t) = 1 - \frac{4.2433a_1}{T[h(t)]}V_\infty G(V_\infty) \tag{38}$$

B.3 Analysis of $\overline{Q}$

If there is an interval of time $I_{\overline{\beta}} = [a, b]$, in which $\overline{\beta} \geq 0$, then $\overline{Q}$ is obviously negative in

that interval, because all of its terms are negative and $\tilde{W}$ is therefore monotonically decreasing in $I_{\bar{\beta}}$. Its maximum value is then $\tilde{W}(a)$ and its minimum value is $\tilde{W}(b)$.

$\bar{\beta}$ is monotonically decreasing with t since $T(h)$ decreases with t. Indeed,

$$\frac{d\bar{\beta}}{dt} = \frac{4.2433^{*}\, a_1 V_\infty \sin(\theta)}{T^2(h)} \frac{dT(h)}{dt} = -4.2433 \left[\frac{a_1 V_\infty \sin(\theta)}{T(h)} \right]^2 < 0 \tag{39}$$

Since $\bar{\beta}$ is decreasing, if the trajectory lasts long enough, $\bar{\beta}$ will become null at $t = b$, with

$$b = \frac{T_s - 4.2433\, a_1 V_\infty G(V_\infty)}{a_1 V_\infty \sin(\theta)}$$

and then become negative.

As a function of $\tilde{W}$, $\bar{Q}$ corresponds to a downward concave parabola, with discriminant

$$\bar{\Delta} = \bar{\beta}^2 - 4\alpha\delta \tag{40}$$

Obviously, at the instant t = b, at which $\bar{\beta} = 0$, the discriminant is: $\bar{\Delta} < 0$. Then, because of its continuity, $\bar{\Delta}$ will remain negative during *a* certain interval of time after *b*. We denote this interval in which $\bar{\beta} < 0$ and $\bar{\Delta} < 0$ by $I_{\bar{\Delta}} = [b, c]$. In this interval, $\bar{Q}$ still has no real roots and is therefore negative. Since $\tilde{W}'(t)$ is negative, $\tilde{W}(t)$ is monotonically decreasing and its maximum value in the interval $I_{\bar{\Delta}}$ is its value at $t = b$ and its minimum value is its value at $t = c$.

In the interval $I_{\bar{\Delta}}$, $\bar{\Delta}$ is a monotonically increasing function of t because both $\bar{\beta}$ and $\bar{\beta}'$ are negative, while α and δ are independent of t. $\bar{\Delta}$ that started negative at $t = b$, will increase and reach the value 0 when

$$\bar{\beta} = 2\cos(\theta)\sqrt{\frac{C_{D0}}{\pi e AR}}, \tag{41}$$

i.e. when $h = h_\Delta$:

$$h_\Delta = \frac{T_s}{a_1} - 4.2433 V_\infty G(V_\infty) \left[1 - 2\cot(\theta)\sqrt{\frac{C_{D0}}{\pi e AR}} \right]^{-1}$$

If the rectilinear trajectory is long enough that it goes through this altitude, this occurs at the instant t_Δ:

$$t_\Delta = t_i + \frac{(h_\Delta - h_i)}{V_\infty \sin(\theta)} \tag{42}$$

after this instant $\bar{\Delta}$ becomes positive.

B.4 Behavior of $\tilde{W}$ when $\bar{\Delta} > 0$

Let us then consider the situation in which $\bar{\Delta} > 0$. $\bar{Q}$ has then the two real roots

$$\tilde{W}_{\pm} = \frac{1}{2\delta}\left[\bar{\beta} \pm \sqrt{\bar{\Delta}}\right] \tag{43}$$

It is straightforward to show that $\tilde{W}_-$ and $\tilde{W}_+$ are positive and are respectively monotonically decreasing and monotonically increasing functions of time. $\tilde{W}'$ is positive when $\tilde{W}(t)$ is in the interval between these two roots: $I_2(t) = (\tilde{W}_-(t), \tilde{W}_+(t))$ and it is negative in the two intervals outside of the roots: $I_1(t) = \{\tilde{W}(t) < \tilde{W}_-(t)\}$ and $I_3(t) = \{\tilde{W}(t) > \tilde{W}_+(t)\}$.

We shall demonstrate the fundamental fact that if at some time t_1, $\tilde{W}(t_1)$ is in the interval $I_2(t_1)$, then at all later times t_2, $\tilde{W}(t_2)$ is in the interval $I_2(t_2)$. This is shown in the following two theorems.

Theorem 1: If $\tilde{W}$ is in the region $I_2(t_1)$ at some time t_1, there exists no later time t_2 at which it will be in the region $I_3(t_2)$.

Proof: Consider the function F: $F(t) = \tilde{W}(t) - \tilde{W}_+(t)$. Suppose that the contrary of the proposition of the theorem is true, that is, $F(t_1) < 0$ and there exists a later time t_2 at which $F(t_2) > 0$. The continuity of F implies that there exists at least one instant τ, between t_1 and t_2 at which $F(\tau) = 0$. Without loss of generality, τ can be taken to be the last instant at which F is null. The mean value theorem applied to $\tilde{W}$ in the interval $[\tau, t_2]$ then says that there exists an instant t_c such that $\tau < t_c < t_2$ at which

$$\tilde{W}'(t_c) = \frac{\tilde{W}(t_2) - \tilde{W}(\tau)}{t_2 - \tau} \tag{44}$$

Note that the right-hand side of Eq. (44) would be positive when $\tilde{W}(t_2) > \tilde{W}_+(t_2)$ and $\tilde{W}(\tau) > \tilde{W}_+(\tau)$ so that

$$\tilde{W}(t_2) - \tilde{W}(\tau) > \tilde{W}_+(t_2) - \tilde{W}_+(\tau) > 0$$

because $\tilde{W}_+$ is monotonically increasing and $t_2 > \tau$ so that $\tilde{W}_+(t_2) > \tilde{W}_+(\tau)$. However, since $t_c > \tau$ and τ is the last zero of F, $F(t_c) > 0$ so that $\tilde{W}'(t_c) < 0$. There is therefore a contradiction in Eq. (44) which implies that the proposition of the theorem cannot be false.

Theorem 2: If $\tilde{W}$ is in the region $I_2(t_1)$ at some time t_1, there exists no time t_2 at which it will be in the region $I_1(t_2)$.

Proof: Let us define the function F: $F(t) = \tilde{W}(t) - \tilde{W}_-(t)$. If at time t, $\tilde{W}(t) \in I_2(t)$, then $F(t) > 0$, by the definition of the interval I_2. Furthermore, $F'(t) = \tilde{W}'(t) - \tilde{W}'_-(t) > 0$ since $\tilde{W}'(t) > 0$ and $\tilde{W}'_-(t) < 0$. The fact that F is monotonically increasing implies that, if $t_2 > t_1$, $F(t_2) > 0$ when $F(t_1) > 0$. Therefore $\tilde{W}$ always remains in I_2.

B.5 The maximum and minimum values of $\tilde{W}$

The above two theorems can be used to determine the maximum and the minimum values of $\tilde{W}$ as follows. Let $t_2 > t_1$.

Case 1: $\tilde{W}(t_1) \in I_1(t_1)$ and $\tilde{W}(t_2) \in I_1(t_2)$

There is then, no instant of time t_c between t_1 and t_2, at which $\tilde{W}(t_c)$ is in $I_2(t_c)$ since otherwise $\tilde{W}$ would have stayed in I_2 at all times after t_c, contrary to the hypothesis. Since $W(t)$ remained in $I_1(t)$

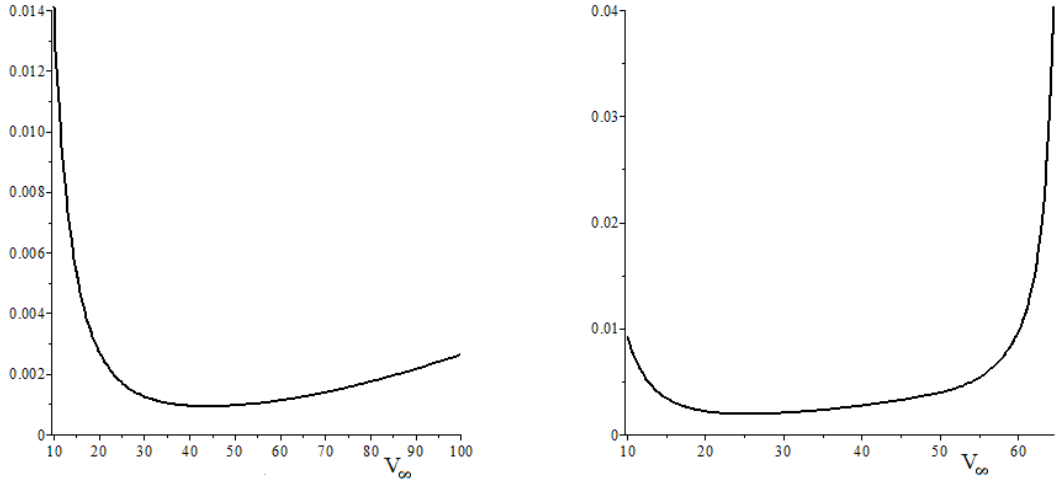

(a) Cessna 182 (b) Silver Fox-like UAV

Fig. 13 Graph of $sin(\theta)$ below which $\bar{Q}(\tilde{W}_i)$ becomes negative, in terms of V_∞

$\forall_t \in [t_1, t_2]$, it was monotonically decreasing $\forall t$. Its maximum value is then its initial value in I_1 and its minimum value is $\tilde{W}_f$.

Case 2: $\tilde{W}(t_1) \in I_1(t_1)$ and $\tilde{W}(t_2) \in I_2(t_2)$

Since $\tilde{W}'(t_1) < 0$ and $\tilde{W}'(t_2) > 0$ while $\tilde{W}'$ is a continuous function of t, there is an instant of time t_0 between t_1 and t_2 at which $\tilde{W}(t_0) = \tilde{W}_-(t_0)$ i.e. $\tilde{W}'(t_0) = 0$ and there is only one such instant of time since once $\tilde{W}$ has entered the region I_2, it cannot thereafter leave that region. In that case $\tilde{W}$ has a single local minimum at $\tilde{W}_-(t_0)$, at which point its slope goes from negative to zero to positive. The minimum value of $\tilde{W}$ is then $\tilde{W}(t_0)$ and its maximum value is either the initial value it had in I_1 or $\tilde{W}_f$. The instant of time t_0 can be determined by finding the instant at which the function F: $F(t) = \tilde{W}(t) - \tilde{W}_-(t)$ becomes null.

Case 3: $\tilde{W}(t_1) \in I_2(t_1)$

In that case, $\tilde{W}(t_2) \in I_2(t_2)$ $\forall$ $t_2 > t_1$. $\tilde{W}$ is monotonically increasing $\forall$ t therefore its minimum value is its initial value in I_2 and its maximum value is $\tilde{W}_f$.

Case 4: $\tilde{W}(t_1) \in I_3(t_1)$ and $\tilde{W}(t_2) \in I_2(t_2)$

The situation is similar to that described in Case 2, with $\tilde{W}_-(t_0)$ replaced by $\tilde{W}_+(t_0)$. $\tilde{W}$ has a single local minimum at $\tilde{W}_+(t_0)$. The minimum value of $\tilde{W}$ is then $\tilde{W}(t_0)$ and its maximum value is either its initial value in I_3 or $\tilde{W}_f$. The instant t_0 can be determined by finding the zero of the function F: $F(t) = \tilde{W}(t) - \tilde{W}_+(t)$.

Case 5: $\tilde{W}(t_1) \in I_3(t_1)$ and $\tilde{W}(t_2) \in I_3(t_2)$

The situation is similar to that described in Case 1. $\tilde{W}$ is monotonically decreasing $\forall t$. Its maximum value is its initial value in I_3 and its minimum value is $\tilde{W}_f$.

B.6 Negativity of $\bar{Q}(\tilde{W}_i)$

The discussion of Section B.5 indicates that the behavior of $\tilde{W}(t)$ can be inferred from the domain in which resides $\tilde{W}(t_i)$. We shall not prove that $\tilde{W}(t_i)$ is always in the domain $I_2(t_i)$, except when the angle θ is very small and we will obtain an expression for these angles. This implies that for all inclinations, except for these very small angles, $\tilde{W}$ is an increasing function of t.

Consider $\bar{Q}$ evaluated at $t = t_i$, in which $cos^2(\theta)$ is replaced by $[1 - sin^2(\theta)]$; the condition $\bar{Q}(W_i) \leq 0$ can then be written as follows:

$$K \sin^2(\theta) - \bar{\beta}_1(t_i)\tilde{W}_i \sin(\theta) - [\alpha + K] \leq 0 \qquad \text{with} \qquad K(V_\infty) = \frac{2}{\pi e A R S V_\infty^2} \tag{45}$$

The left-hand side of Ineq. (45) is a quadratic expression in $sin(\theta)$, which corresponds to an upward concave parabola. Its discriminant is positive, it has two real roots, the smallest of which is negative since the intercept of the parabola on the ordinate is negative. Thus, Ineq. (45) is satisfied if and only if $sin(\theta)$ is smaller than the largest root, that is

$$sin(\theta) \leq \frac{1}{2K}\left\{\bar{\beta}_1(t_i)\tilde{W}_i + \sqrt{\left[\bar{\beta}_1(t_i)\tilde{W}_i\right]^2 + 4K[\alpha + K]}\right\} \tag{46}$$

Fig. 13 shows the curve of $sin(\theta)$ as a function of V_∞, below which $\bar{Q}(\tilde{W}_i)$ becomes negative, for the Cessna 182 and the Silver Fox-like UAV. The largest angle at which $\bar{Q}(\tilde{W}_i)$ can be negative is seen to be 0.8° for the Cessna 182 and 2.3° for the Silver Fox-like UAV. For all trajectories more inclined than these angles, $\tilde{W}$ will be a monotonically increasing function of t.